Relative contribution of cationic surfactant and counter-anion to a liquid film tension

Chi M. Phan[a] and Muhammad Haseeb[a]

Discipline of Chemical Engineering and Institute of Functional Molecules and Interfaces, Curtin University, Perth, WA 6845, Australia

Corresponding author: c.phan@curtin.edu.au

Abstract

A model was developed to predict the bubble deformation in the presence of a charged surface. The model was successfully verified with a bubble containing a cationic surfactant, cetyltrimethylammonium bromide. The modelling results revealed that the film tension linearly increased with the distance from the charged surface, due to the electrostatic repulsion of the anions. More importantly, the analysis demonstrated that hydrated Br^- increased film tension, whereas surfactant molecules reduced film tension. The anion's increment was estimated at ~ 14% of the surfactant's reduction. The results verified the contrasting influences of surfactant and its counter-ions on the tension of the air/liquid interfacial layer.

Keywords: film tension, ionic interaction, cationic surfactant

Introduction

Surfactants-stabilized foams are found in many industrial [1] and natural processes [2]. The foaming fractionation process can be employed to separate the dissolved ions by interaction with ionic surfactants [3,4]. In the literature, the interfacial adsorption of surfactant and counter-ion is often simplified into a single dividing plane [5]. On the other hand, theoretical and experimental studies have revealed different roles of surfactant and counter-ions within the interfacial zone. It

has been shown that ions are located further from the surface,[6] with a strong hydration shell [7] and a lower frequency of H-bonds switching [8]. The hydrated counter-ions affect the surface tension via their interaction with H-bond networks in the sub-surface layer [9]. The selective impact of counter-ions on the surface layer has been well-documented for cationic surfactants [10], such as C_{14}TACl/C_{14}TABr[11,12] and C_{16}TACl/C_{16}TABr [13]. The anions adsorption varies with atomic size as well as water surface layer [7,14]. Similarly, the anionic surfactant can have distinguished interactions with both monovalent [3] and divalent cations [4].

From these results, it can be hypothesized that the surfactant and counter-ion have unequal contributions to the surface tension. In a recent simulation study, the contribution of surfactant and counter-ion to surface tension was quantified separately [15]. It is fascinating to note that a cationic surfactant, dodecyl trimethyl ammonium, and its counter-anion have opposite contributions to surface tension. The unequal and contrasting contributions have a significant ramification on the fundamental understanding and applications of ionic surfactants.

To quantify the individual impacts of counter-ions and surfactants, the interfacial layer needs to be assessed at non-neutral conditions. The non-neutral conditions of the air/water surface have been obtained under dynamic conditions. For instance, it has been demonstrated that the interfacial layer can be divided into an “immobile” layer of hydrophobic tails,[16] and a “mobile” layer dominated by the hydrated counter-ions. A simulation study also verified that the hydrate counter-ions have much higher diffusivity than surfactant molecules [17]. The clearest evidence of the multi-layers structure was obtained for the amphiphilic polymer at the air/water surface [18]. The separation between these two layers at the air/water surface is often evidenced via the zeta potential of small air bubbles [19]. However, these dynamic conditions are not suitable for surface tension

quantification. Furthermore, these investigations focuses on the air/water surface with a large bulk liquid phase.

This study aims to generate and quantify the tension at a non-neutral and static state. Hence, we focus on the thin film of a bubble, which is easily affected by an electrical force [20]. The local non-neutral condition can generate a variable film tension, which then can be optically captured and mathematically quantified via the classical Young-Laplace equation [21]. Ultimately, the study aims to provide some quantitative measurements on the relative contribution of surfactant and its counter-ion to the surface tension.

Theory

To obtain the static, and yet non-neutral, conditions of the surfactant layer, a bubble film was employed under an electrostatic field (Figure 1a). A model is developed and solved numerically for a bubble shape, which is deformed via non-neutral distribution within the film. The shape of an axisymmetric interface can be described by a system of three 1st ODEs:[21]

$$\frac{dx}{ds} = \cos\phi \tag{1}$$

$$\frac{dz}{ds} = \sin\phi \tag{2}$$

$$\frac{d\phi}{ds} + \frac{\sin\phi}{x} = \frac{\Delta P}{\gamma(z)} \tag{3}$$

Where s is arc length measure from initial point, ϕ is the tangent angle, γ is the interfacial tension and ΔP is the pressure difference.

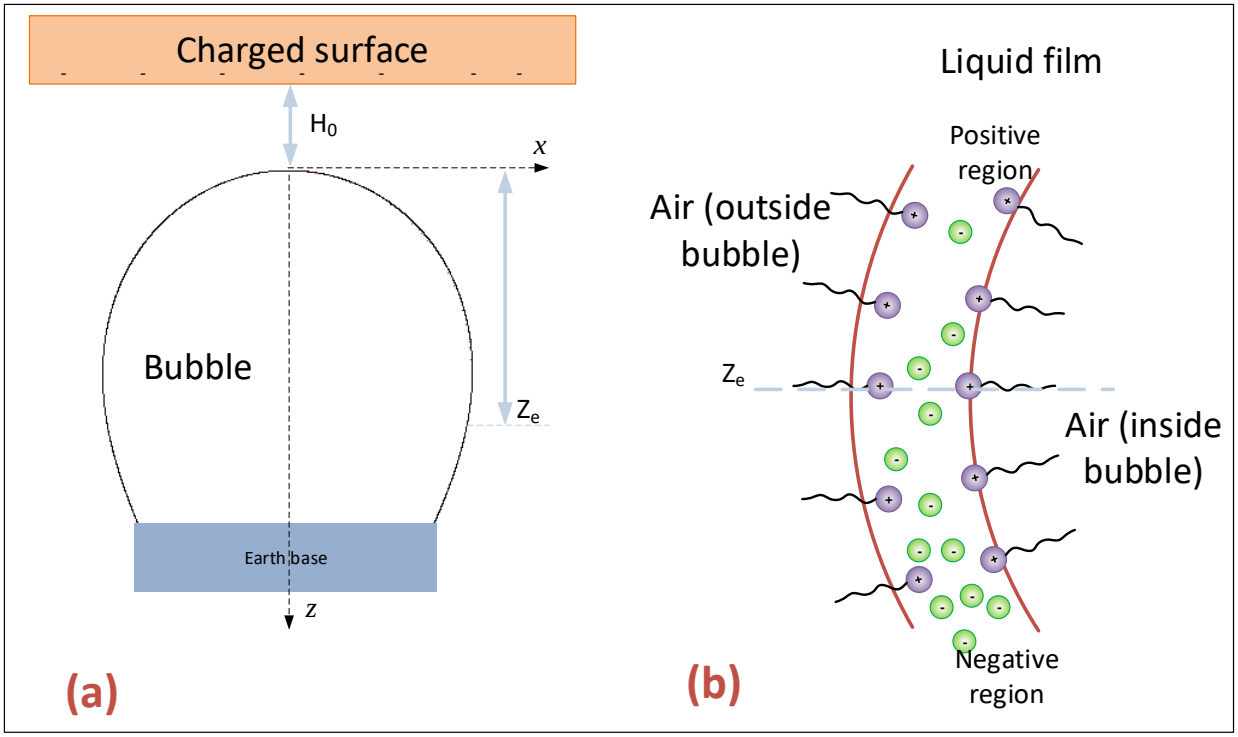

Figure 1. Bubble deformation under external electrostatic force (a) geometry of the bubble, (b) a non-uniform distribution of anions along z-axis.

The above system of ODEs has been solved for constant γ, producing shape-based methods for tension determination. The axis-symmetric interface can be a pendant or sessile shape in the conventional drop/bubble [22], or a holm shape for a large interface [23]. For the soap bubble in this study, however, the pressure difference is constant, and the tension is variable with z-axis (Figure 1b). In this instance, the thin liquid film is supported by the interfacial tension, instead of a solid frame as in the flat soap film [24]. The initial conditions of the above equations are defined at the apex of the bubble (when x=0 and z=0):

$$\phi_0 = 0 \qquad (4)$$

In the absence of an external force, the film tension, γ_e , is uniform throughout the bubble shape, which is a part of a perfect sphere [25]. The value of γ_e is determined as twice of the surface tension [26].

In the presence of an external electrostatic field, the hydrated counter-ions are affected by the electrical force. On the other hand, the surfactant molecules are more immobile due to adsorption at the air/liquid surface. In the case of the electrostatic field from the surface of an insulator (Figure 1), distanced at H_0 from the apex, the local acting force is inversely proportional to the distance, that is $z+H_0$. This force is balanced by electrostatic binding between the surface heads and counter-ions [27]. Hence, there is an ionic gradient in the z-axis. Since the film is neutral as the whole, there is a distance from the apex, Z_e, at which the thin film is neutral. At this distance, the film tension should be the same as γ_e. Above Z_e, the film is positively charged, that is having fewer counter-ions than surfactant head. Below Z_e, the film is negatively charged.

Since there is no prior model on the relationship between the local charge and film tension, we assume a linear correlation. Furthermore, the two correlations, below and above Z_e, should be different due to the unequal contribution of anion and surfactant to the film tension. Both correlations equal unity at $z = Z_e$. The equation satisfies these condition is given by:

$$\frac{\gamma(z)}{\gamma_e} = (1-b_1)\frac{z+H_0}{Z_e+H_0} + b_1 \qquad \text{for } z < Z_e \qquad (5)$$

$$\frac{\gamma(z)}{\gamma_e} = (1-b_2)\frac{z+H_0}{Z_e+H_0} + b_2 \qquad \text{for } z > Z_e$$

Where b_1 and b_2 are the dimensionless constant for two regions.

It can be seen that when both b_1 and b_2 equal to 1, the above equation reduces to constant tension, that is $\gamma(z)$ equals to γ_e for the whole bubble. Substituting Eq(7) into Eq.(3), one has:

$$\frac{\mathrm{d}\phi}{\mathrm{d}s}+\frac{\sin\phi}{x}=\frac{\Delta \mathrm{P}}{\gamma_{\mathrm{e}}}\Big/\left((1-b_1)\frac{z+\mathrm{H}_0}{Z_{\mathrm{e}}+\mathrm{H}_0}+b_1\right) \qquad \text{for } z < Z_e \qquad (6)$$

$$\frac{\mathrm{d}\phi}{\mathrm{d}s}+\frac{\sin\phi}{x}=\frac{\Delta \mathrm{P}}{\gamma_{\mathrm{e}}}\Big/\left((1-b_2)\frac{z+\mathrm{H}_0}{Z_{\mathrm{e}}+\mathrm{H}_0}+b_2\right) \qquad \text{for } z > Z_e$$

The system of Eq.(1), (2) and (6) can be solved simultaneously [28]. The obtained interface is fitted with the experimental images for different H_0, which was directly determined from the experimental conditions. The value of $\Delta P/\gamma_e$ can be easily obtained from a non-charged bubble, which is a part of a sphere. Consequently, the model has three adjustable parameters: Z_e , b_1 and b_2.

Experimental

Teflon was selected as the insulator due to its high surface triboelectric affinity, at -190 nC/J [29]. The surface was charged by rubbing Teflon surface against a cloth. The electrostatic charge was verified by a surface voltmeter (SVM2, Alpha Lab Inc.). The saturated surface charge was obtained at -19.7 kV± 2%, with respect to the ground, at a distance of 2.54 cm. This value presents a static electrical field of 300 to 400 V/m, which is in a similar order of electro-driven interfacial deformation [30]. An aqueous solution of cetyltrimethylammonium bromide (CTAB) and glycerol was selected to stabilize the bubble during the deformation [31]. The surfactant concentration was twice the critical micelle concentration [32], at 2 mM. From a previous study, it was found that at low concentration, especially below CMCs, the soap film is very unstable and does not allow

112 effective observations [25]. Consequently, 2 mM was selected to ensure the film stability. The
113 glycerol concentration was kept at 10% by weight. The equilibrium surface tension was measured
114 by the pendant drop method [33], and equaled to 30.7 mN/m.

115 A bubble was formed by injecting air onto a plastic cup with a diameter of 12.6 mm. Subsequently,
116 the charged Teflon surface was gradually moved closer to the bubble. If the charged Teflon surface
117 was moved too close or too fast, the bubble forms a cone shape. Subsequently, a small liquid bridge
118 was formed and detached from the bubble. The formation of a liquid bridge has been reported
119 previously under a high electrical field [34]. In our system, the formation of the cone shape,
120 detachment of small liquid bridge and bubble restoration, happened within 20 milliseconds. Such
121 dynamic behavior was only obtainable with a high-speed camera. An example of the process
122 (captured by a FASTCAM SA4 model 500K-M3) is showed in Figure 2. The image sequence
123 demonstrated the fast ion separation and movement, within milliseconds. Consequently, it is
124 expected that ionic rearrangement within the thin film reached the equilibrium quickly for non-
125 bursting conditions.

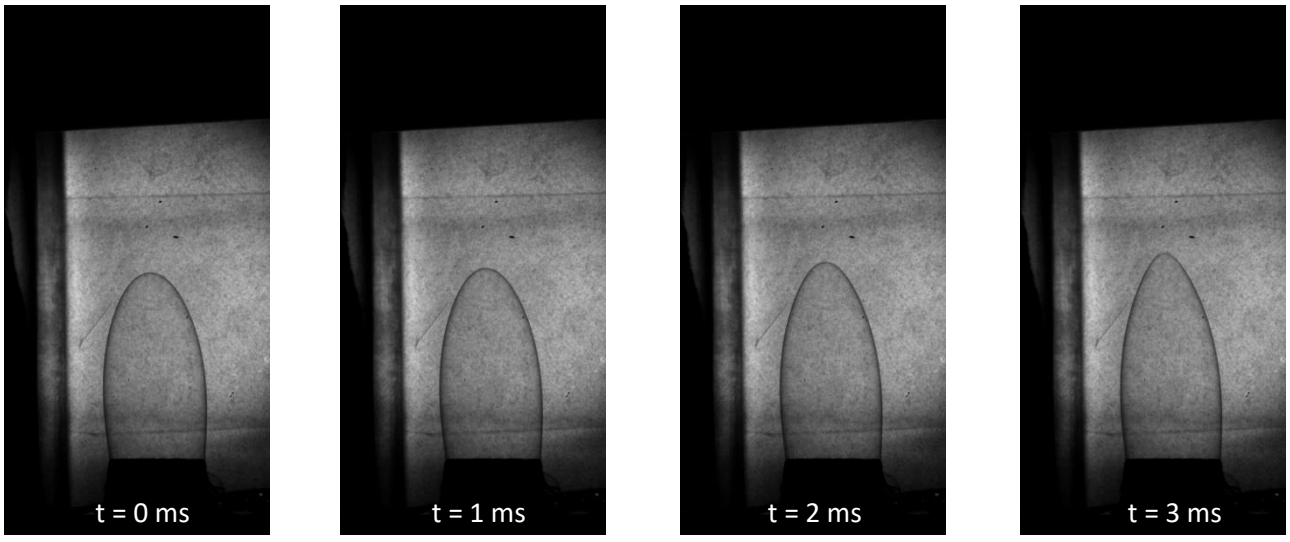

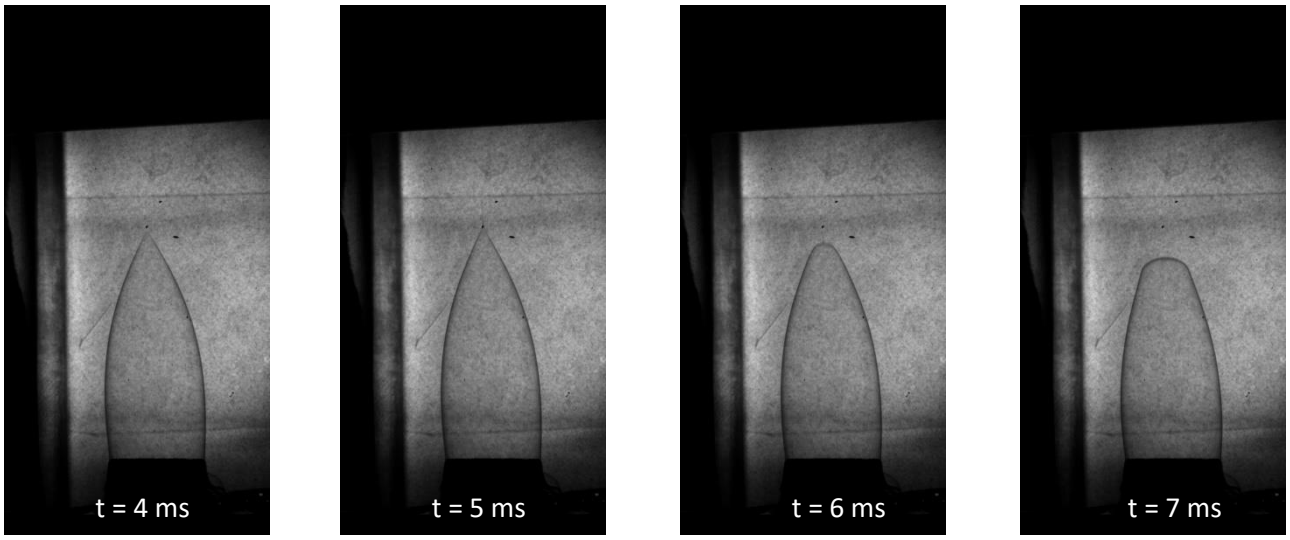

Figure 2. Dynamic deformation of the bubble, captured with a high-speed camera at 1000 frame-per-second.

The minimum distance for the non-bursting condition was ~ 21 mm. Consequently, moderate distances, $H_0 > 21$ mm, was employed for the model validation. The bubble shape was captured using a digital camera at a resolution of 5184 × 3456 pixels for image analysis.

Results and Discussion

The bubble shapes at different distance H_0 are shown in Figure 3. It can be seen that the deformation, that is vertical prolongation, increased with the decreasing H_0. Notably, the radius of curvature at the apex of the deformed bubble was smaller than the middle region. The reduced principle radius indicated quantitatively that the film tension at the apex was smaller than that in the middle region, which means b_1 is smaller than 1.

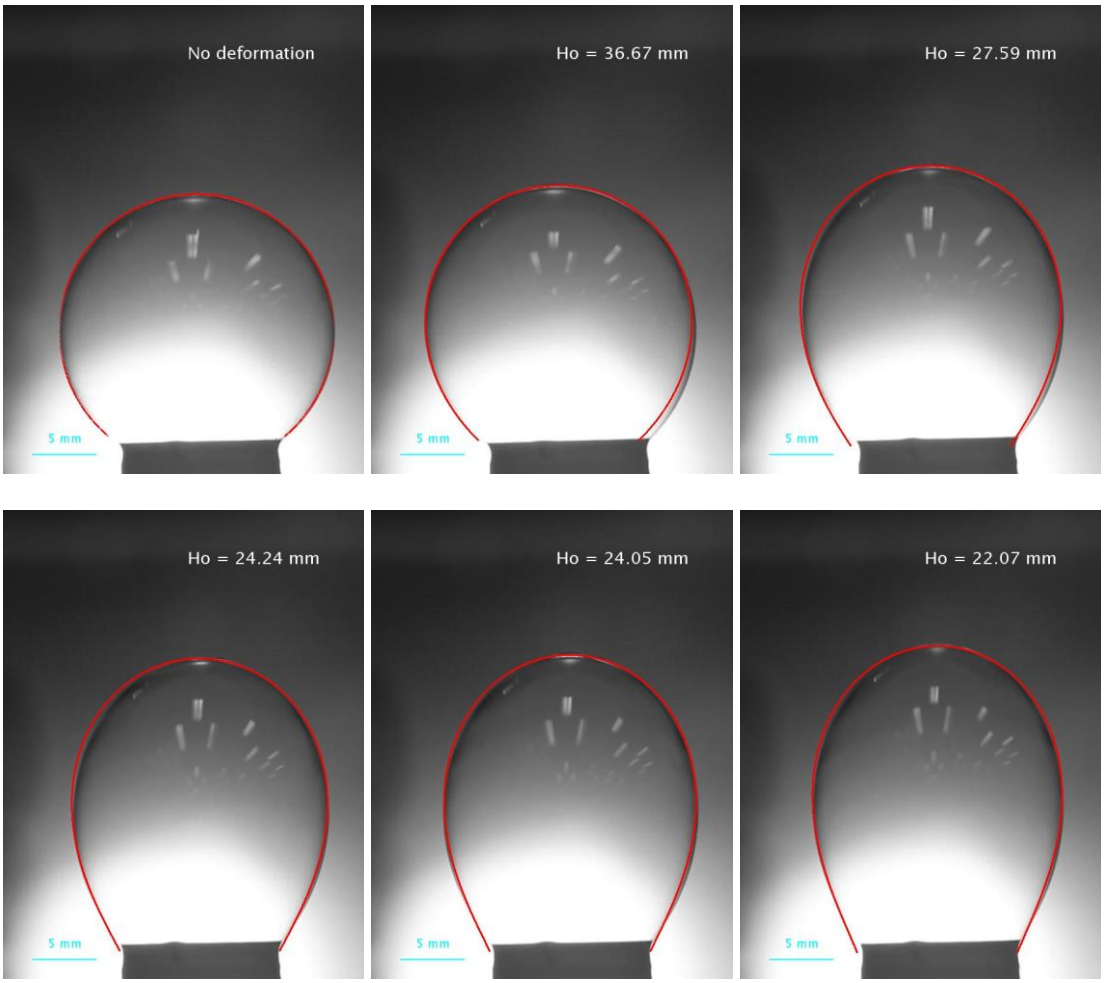

Figure 3. Bubble deformation: experimental images and modelled prediction (red curve) at different H_0.

The modelling was applied to each bubble shape to determine out the corresponding values of the three fitting parameters. In addition to the best-fitted values, the model can predict the bubble shape at different values of Z_e (Figure 4).

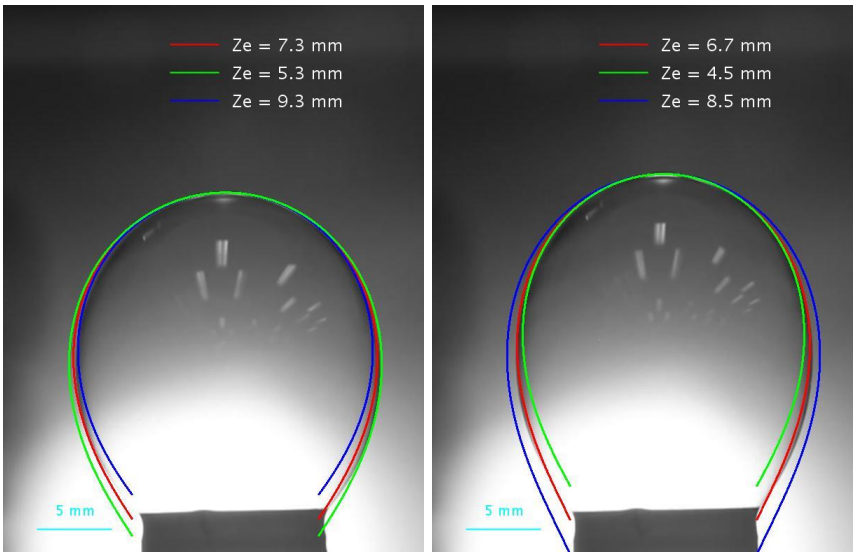

Figure 4. Influence of Z_e on the shape of bubble: (left) H_0=27.59 mm and (right) H_0=24.05 mm (red curves are best-fitted)

The best-fitting values are plotted in Figure 5 as function of H_0. The value of Z_e follows a linear correlation with H_0. The linearity is physically consistent with the electrostatic field: the position of neutral charge is pushed further down as the charged surface moves closer. As H_0 approaches infinite, both b_1 and b_2 approach unity as expected. As H_0 approaches the limitation of 21 mm, both b_1 and b_2 were reduced. The decreasing trends of b_1 and b_2 (between 0 and 1), indicate a higher slope of the ionic gradient. It is noteworthy that b_1 was dramatically dropped to zero as H_0 ~ 21 mm. Qualitatively, the trends are consistent with the increasing strength of the electrostatic field.

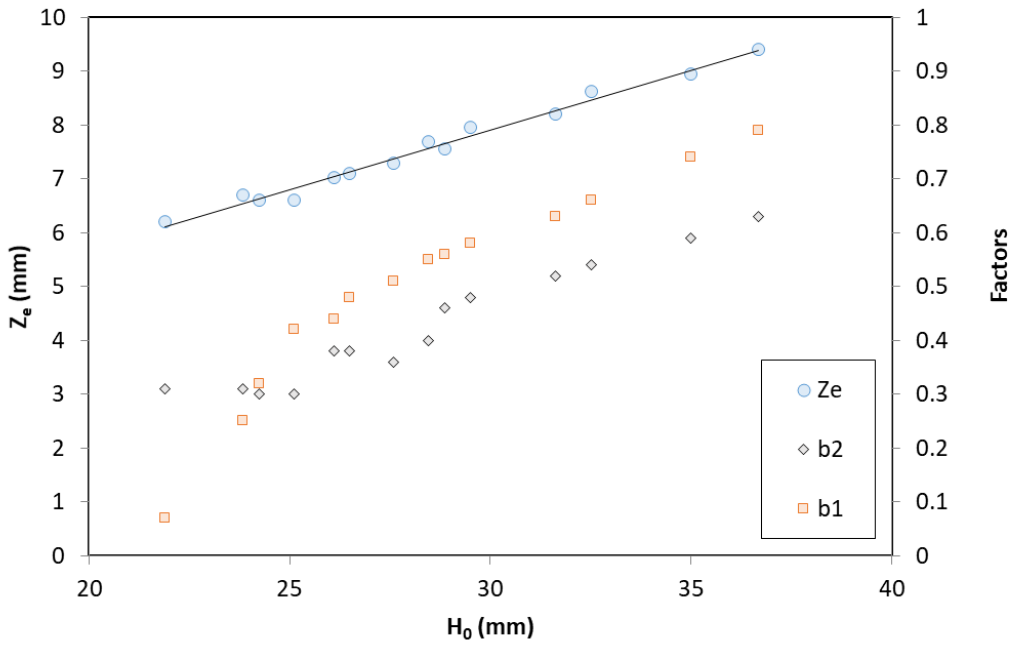

156

157 Figure 5. Model parameters as functions of H_0.

158 The model validates that the non-neutral conditions can be maintained at equilibrium. The
159 inequality between the surfactant and its counter-ion generate the variable tension. While the local
160 ionic gradient within the thin film is unknown, the film tension is variable with distance as plotted
161 in Figure 6. The value of the film tension is lower at the apex, which contains fewer anions. As
162 distance H_0 is reduced, the anion concentration at the apex is gradually reduced. Qualitatively, the
163 trend indicates that Br^- has a positive impact on the film tension.

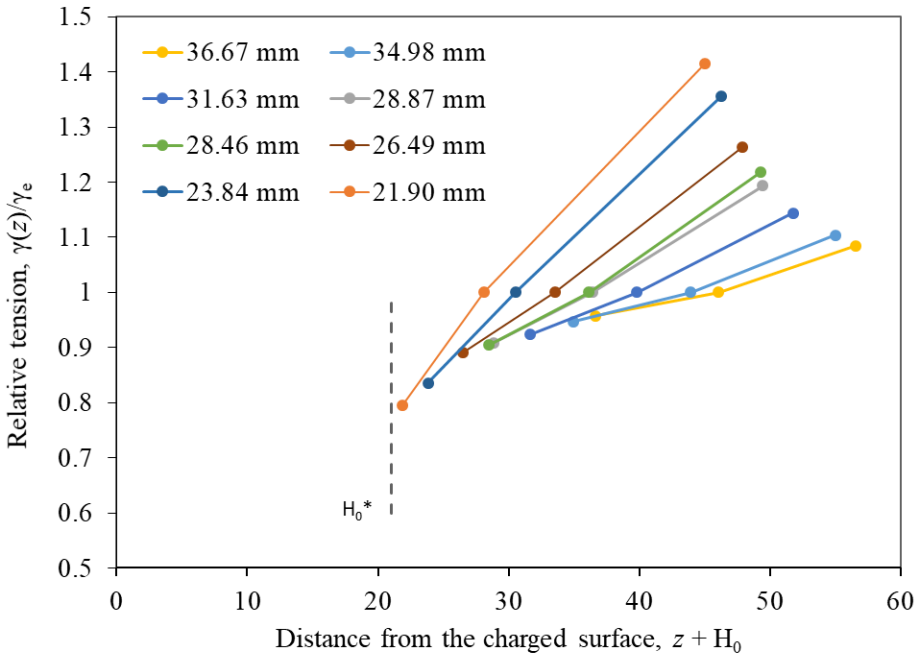

164

165 Figure 6. Relative tension as a function of H_0. Each line represents the tension profile of a bubble
166 shape (the three points along each line represent the positions of the apex, the neutral point and
167 base of the bubble, respectively).

168 To quantify the individual impacts of anion and surfactant, a critical separating distance is
169 considered. It has been showed that the ionic pairing of counter-ion with the adsorbed surfactant
170 are variable with the electrostatic strength. For instance, the binding varied with the space length
171 the cationic Gemini surfactants,[35] and the hydration shell of the anion [36]. Hence, it is expected
172 that the anions can be completely displaced by a sufficiently strong electrostatic field.
173 Consequently, there is a critical distance, H_0 *, at which the liquid film at the apex has no free
174 anions. Further decrement of H_0 would break the liquid film and form a charge liquid bridge as in
175 Figure 2. From the high-speed images and Figure 5, it can be estimated that the value of H_0* for
176 the studied system is ~ 21 mm. At this distance, the film tension, γ^*, at the apex is dominated by
177 surfactant molecules solely. It should be noted that the value of H_0* is dependent on the surfactant
178 system and surface charge. A lower charge density or lower surfactant packing will increase the

179 distance. Teflon was one of the highest insulators. From the static voltage of -19.7 kV, the charge
180 density of Teflon plate is calculated at 0.7×10^{-6} mol/m^2. Similar, CTAB is strongest cationic
181 surfactants, with saturated adsorption ~ 3×10^{-6} mol/m^2[37]. The critical distance is also influenced
182 by the bubble size: a smaller bubble will have higher ΔP and smaller H_0*. As the results, the critical
183 distance for the studied system was sufficient small for optical observation. The slope between the
184 apex and the neutrally charged position, H_0*+Z_e*, was highest at this distance (Figure 5). This
185 critical gradient can be estimated at the practically obtainable distance of H_0 = 21.9 mm. Hence,
186 the value of γ^*/γ_e is estimated at 79%.

187 The surface tension, or film tension, is dominated by the H-bonds of water molecules [38]. In the
188 presence of cationic surfactants, both surfactant and hydrated anions reduce the surface tension by
189 disrupting the interfacial H-bonds of water surface. While the alkyl tails directly disrupt the water
190 layer [39], the hydrated anions affects the tension via the interaction of hydration shells [40–42].
191 Quantitatively, the reduction in film tension is given by:

192 $$\gamma_0 - \gamma(z) = \varepsilon_s \Gamma_s(z) + \varepsilon_a \Gamma_a(z) \quad (7)$$

193 Where γ_0 is the film tension of pure solvent (144 mN/m); ε_s and ε_a are the molecular impact of the
194 surfactant and hydrated anion, respectively; $\Gamma_s(z)$ and $\Gamma_a(z)$ are the local adsorption concentrations
195 of surfactant and anion, respectively.

196 Since the surfactant adsorption is governed by hydrophobic force, it can be assumed that Γ_a remains
197 constant. At the neutrally charged position, H_0*+Z_e*, $\Gamma_a = \Gamma_s$. At H_0*, there is no free anions at the
198 apex. Assuming a complete ionic separation, one can expect $\Gamma_a = 0$ at the apex. Applying Eq.(7) to
199 these two positions, the ratio between ε_s and ε_a can be determined as:

$$\frac{\varepsilon_a}{\varepsilon_s} = -0.14 \quad (8)$$

The negative sign indicated that Br^- has an opposite contribution to surfactant. The results are consistent with a simulation study on the individual influence on the surface tension [15]. The positive contribution of Br^- to the film tension is also consistent with the increased surface tension by halide salts [43–45]. The study can be extended to anionic surfactant systems, which is important for cations removal [4], with a positively charged surface.

Conclusions

The soap film tension gradient is experimentally observed under an electrostatic equilibrium. It was revealed that the surfactant layer and counter-ions can be separated locally and have a significant effect at the micro-scale. The modelling results verified some quantitative assessment of the thin film. The surfactant and anion have opposite contributions to the film tension. While surfactant reduces the tension, anion increases the tension. For the studied system, the impact of the anion is much weaker (~14%) than that of the surfactant and thus is cancelled out.

It should be noted that the tension-induced surface deformation has been reported as the famous "tear of wine" or Marangoni phenomena. In the instance, the variable surface tension was caused by the composition gradient along the surface, which was maintained dynamically. On contrast, the obtained gradient in this study was generated by a static displacement between anion and surfactant. Finally, it is interesting to note that the bubble can be busted by a charged object without direct contact. The method can be extended to explore the molecular structure of the interfacial layer and control the foam stability. A routine software combining image analysis and numerical modelling will be useful for soap film analysis. Such modelling program can be applied *in-situ* to

provide timely insights into the composition of foaming films, which is variable during industrial processes.

Acknowledgement

The authors acknowledge RimstarOrg for an illustrative demonstration of the bubble deformation on Youtube (https://www.youtube.com/watch?v=aySWX55-xX4).

References

[1] L.K. Koopal, T. Goloub, A. De Keizer, M.P. Sidorova, The effect of cationic surfactants on wetting, colloid stability and flotation of silica, Colloids Surfaces A Physicochem. Eng. Asp. 151 (1999) 15–25. doi:10.1016/S0927-7757(98)00389-6.

[2] S. Tcholakova, F. Mustan, N. Pagureva, K. Golemanov, N.D. Denkov, E.G. Pelan, S.D. Stoyanov, Role of surface properties for the kinetics of bubble Ostwald ripening in saponin-stabilized foams, Colloids Surfaces A Physicochem. Eng. Asp. 534 (2017) 16–25. doi:10.1016/j.colsurfa.2017.04.055.

[3] K. Matsuoka, H. Miura, S. Karima, C. Taketaka, S. Ouno, Y. Moroi, Removal of alkali metal ions from aqueous solution by foam separation method, J. Mol. Liq. 263 (2018) 89–95. doi:10.1016/j.molliq.2018.04.136.

[4] K. Matsuoka, S. Hasegawa, T. Yuma, Y. Goto, Application of foam separation method for removal of alkaline earth metal ions from solution, J. Mol. Liq. 294 (2019) 111663. doi:10.1016/j.molliq.2019.111663.

[5] J. Eastoe, J.S. Dalton, Dynamic surface tension and adsorption mechanisms of surfactants at the air-water interface, Adv. Colloid Interface Sci. 85 (2000) 103–144. doi:10.1016/S0001-8686(99)00017-2.

[6] H. Tissot, G. Olivieri, J.J. Gallet, F. Bournel, M.G. Silly, F. Sirotti, F. Rochet, Cation Depth-Distribution at Alkali Halide Aqueous Solution Surfaces, J. Phys. Chem. C. 119 (2015) 9253–9259. doi:10.1021/jp512695c.

[7] C. V. Nguyen, C.M. Phan, H. Nakahara, O. Shibata, Surface structure of sodium chloride solution, J. Mol. Liq. 248 (2017) 1039–1043. doi:10.1016/j.molliq.2017.10.138.

[8] I.A. Heisler, S.R. Meech, Low-frequency modes of aqueous alkali halide solutions: Glimpsing the hydrogen bonding vibration, Science (80-.). 327 (2010) 857–860. doi:10.1126/science.1183799.

[9] G. Gao, C. V. Nguyen, C.M. Phan, Molecular arrangement between electrolyte and alcohol at the air/water interface, J. Mol. Liq. 242 (2017) 859–867. doi:10.1016/j.molliq.2017.07.083.

[10] M.J. Rosen, J.T. Kunjappu, Surfactants and interfacial phenomena, Wiley, 2012.

[11] S. Durand-Vidai, M. Jardat, V. Dahirel, O. Bernard, K. Perrigaud, P. Turq, Determining the radius and the apparent charge of a micelle from electrical conductivity measurements by using a transport theory: Explicit equations for practical use, J. Phys. Chem. B. 110 (2006) 15542–15547. doi:10.1021/jp062956n.

[12] K.K. Sharker, S. ichi Yusa, C.M. Phan, Micellar formation of cationic surfactants, Heliyon. 5 (2019) e02425. doi:10.1016/j.heliyon.2019.e02425.

[13] C. Zhang, T. Geng, Y. Jiang, L. Zhao, H. Ju, Y. Wang, Impact of NaCl concentration on equilibrium and dynamic surface adsorption of cationic surfactants in aqueous solution, J. Mol. Liq. 238 (2017) 423–429. doi:10.1016/j.molliq.2017.05.033.

[14] C. V. Nguyen, H. Nakahara, O. Shibata, C.M. Phan, Adsorption of sodium iodine at air/water interface, J. Mol. Liq. (2019) 112076. doi:10.1016/j.molliq.2019.112076.

[15] G. Hantal, M. Sega, G. Horvai, P. Jedlovszky, Contribution of Different Molecules and Moieties to the Surface Tension in Aqueous Surfactant Solutions, J. Phys. Chem. C. (2019) acs.jpcc.9b02553. doi:10.1021/acs.jpcc.9b02553.

[16] B. Blanc, O. Bonhomme, P.F. Brevet, E. Benichou, C. Ybert, A.L. Biance, Electroosmosis near surfactant laden liquid-air interfaces, Soft Matter. 14 (2018) 2604–2609. doi:10.1039/c7sm02508d.

[17] N.A. Volkov, B.B. Divinskiy, P.N. Vorontsov-Velyaminov, A.K. Shchekin, Diffusivities of species in ionic micellar solutions: Molecular dynamic simulation, Colloids Surfaces A Physicochem. Eng. Asp. 480 (2015) 165–170. doi:10.1016/j.colsurfa.2014.10.030.

[18] E. Mouri, Y. Furuya, K. Matsumoto, H. Matsuoka, Hydrophilic chain length dependence of the ionic amphiphilic polymer monolayer structure at the air/water interface, Langmuir. 20 (2004) 8062–8067. doi:10.1021/la049256z.

[19] M. Manciu, F.S. Manciu, E. Ruckenstein, On the surface tension and Zeta potential of electrolyte solutions, Adv. Colloid Interface Sci. 244 (2017) 90–99. doi:10.1016/j.cis.2016.06.006.

[20] L.A. Del Castillo, S. Ohnishi, S.L. Carnie, R.G. Horn, Variation of Local Surface Properties of an Air Bubble in Water Caused by Its Interaction with Another Surface, Langmuir. 32 (2016) 7671–7682. doi:10.1021/acs.langmuir.6b01949.

[21] E.A. Boucher, Reports on Progress in Physics Capillary phenomena: Properties of systems with fluid/fluid interfaces Capillary phenomena: properties of systems with fluidlfluid interfaces, Rep. Prog. Phys. Rep. Prog. Phys. 43 (1980). http://iopscience.iop.org/article/10.1088/0034-4885/43/4/003/pdf (accessed March 28, 2018).

[22] A.J. Prosser, E.I. Franses, Adsorption and surface tension of ionic surfactants at the air-water interface: Review and evaluation of equilibrium models, Colloids Surfaces A Physicochem. Eng. Asp. 178 (2001) 1–40. doi:10.1016/S0927-7757(00)00706-8.

[23] A. Hyde, C. Phan, G. Ingram, Determining liquid–liquid interfacial tension from a submerged meniscus, Colloids Surfaces A Physicochem. Eng. Asp. 459 (2014) 267–273. doi:http://dx.doi.org/10.1016/j.colsurfa.2014.07.016.

291 [24] P.G. De Gennes, “Young” soap films, Langmuir. 17 (2001) 2416–2419. doi:10.1021/la001538l.

292 [25] C.V. Nguyen, S.-I. Yusa, C.M. Phan, Stability of aqueous film with a photo-responsive surfactant, J.
293 Chem. Eng. Japan. 49 (2016). doi:10.1252/jcej.15we290.

294 [26] S. Sett, S. Sinha-Ray, A.L. Yarin, Gravitational drainage of foam films, Langmuir. 29 (2013) 4934–
295 4947. doi:10.1021/la4003127.

296 [27] N.A. Volkov, A.K. Shchekin, N. V. Tuzov, T.S. Lebedeva, M.A. Kazantseva, Molecular modeling of
297 ionic aggregates at several concentrations of SDS in aqueous solution, J. Mol. Liq. 236 (2017)
298 414–421. doi:10.1016/j.molliq.2017.04.018.

299 [28] C.M. Phan, Stability of a floating water droplet on an oil surface, Langmuir. 30 (2014).
300 doi:10.1021/la403830k.

301 [29] B.W. Lee, D.E. Orr, The Triboelectric Series - AlphaLab, Inc, (n.d.).
302 https://www.alphalabinc.com/triboelectric-series/ (accessed August 22, 2019).

303 [30] W.D. Ristenpart, J.C. Bird, A. Belmonte, F. Dollar, H.A. Stone, Non-coalescence of oppositely
304 charged drops, Nature. 461 (2009) 377–380. doi:10.1038/nature08294.

305 [31] F. Elias, S. Kosgodagan Acharige, L. Rose, C. Gay, V. Leroy, C. Derec, Vibration of soap films and
306 Plateau borders, as elementary blocks of a vibrating liquid foam, Colloids Surfaces A
307 Physicochem. Eng. Asp. 534 (2017) 85–93. doi:10.1016/j.colsurfa.2017.02.091.

308 [32] C.M. Phan, T.N. Le, S. ichi Yusa, A new and consistent model for dynamic adsorption of CTAB at
309 air/water interface, Colloids Surfaces A Physicochem. Eng. Asp. 406 (2012) 24–30.
310 doi:10.1016/j.colsurfa.2012.04.044.

311 [33] Y.Y. Zuo, M. Ding, A. Bateni, M. Hoorfar, A.W. Neumann, Improvement of interfacial tension
312 measurement using a captive bubble in conjunction with axisymmetric drop shape analysis
313 (ADSA), in: Colloids Surfaces A, Elsevier, 2004: pp. 233–246. doi:10.1016/j.colsurfa.2004.04.081.

314 [34] V. Anand, S. Roy, V.M. Naik, V.A. Juvekar, R.M. Thaokar, Electrocoalescence of a pair of
315 conducting drops in an insulating oil, J. Fluid Mech. 859 (2019) 839–850.
316 doi:10.1017/jfm.2018.849.

317 [35] Y. Geng, L.S. Romsted, F. Menger, Specific ion pairing and interfacial hydration as controlling
318 factors in gemini micelle morphology. Chemical trapping studies, J. Am. Chem. Soc. 128 (2006)
319 492–501. doi:10.1021/ja056807e.

320 [36] P. Koelsch, H. Motschmann, Varying the counterions at a charged interface, Langmuir. 21 (2005)
321 3436–3442. doi:10.1021/la0480179.

322 [37] C.M. Phan, T.N. Le, C. V. Nguyen, S.I. Yusa, Modeling adsorption of cationic surfactants at
323 air/water interface without using the gibbs equation, Langmuir. 29 (2013) 4743–4749.
324 doi:10.1021/la3046302.

325 [38] Y. Fan, X. Chen, L. Yang, P. Cremer, Y.Q. Gao, On the structure of water at the aqueous/air
326 interface, J. Phys. Chem. B. 113 (2009) 11672–11679. doi:10.1021/jp900117t.

327 [39] C.M. Phan, Dissociation of Ionic Surfactants at the Air/Water Interface: Complete or Partial?, J.

328 Phys. Chem. B. 120 (2016) 7681–7686. doi:10.1021/acs.jpcb.6b06074.

329 [40] L.X. Dang, G.K. Schenter, C.D. Wick, Rate Theory of Ion Pairing at the Water Liquid–Vapor
330 Interface, J. Phys. Chem. C. 121 (2017) 10018–10026. doi:10.1021/acs.jpcc.7b02223.

331 [41] N.B. Vargaftik, B.N. Volkov, L.D. Voljak, International Tables of the Surface Tension of Water, J.
332 Phys. Chem. Ref. Data. 12 (1983) 817–820. doi:10.1063/1.555688.

333 [42] C.M. Phan, C. V. Nguyen, S.I. Yusa, N.L. Yamada, Synergistic adsorption of MIBC/CTAB mixture at
334 the air/water interface and applicability of gibbs adsorption equation, Langmuir. 30 (2014) 5790–
335 5796. doi:10.1021/la500721d.

336 [43] O. Ozdemir, S.I. Karakashev, A. V. Nguyen, J.D. Miller, Adsorption and surface tension analysis of
337 concentrated alkali halide brine solutions, Miner. Eng. 22 (2009) 263–271.
338 doi:10.1016/j.mineng.2008.08.001.

339 [44] L. Onsager, N.N.T. Samaras, The Surface Tension of Debye-Hückel Electrolytes, J. Chem. Phys. 2
340 (1934) 528–536. doi:10.1063/1.1749522.

341 [45] M. Boström, D.R.M. Williams, B.W. Ninham, Surface tension of electrolytes: Specific ion effects
342 explained by dispersion forces, Langmuir. 17 (2001) 4475–4478. doi:10.1021/la0102298.

343